

---

Article

Not peer-reviewed version

---

# Sustainable Use of Gypsum Waste for Applications in Soil-Cement Bricks: Mechanical, Environmental, and Durability Performance

---

[Elvia Soraya Santos Nascimento](#) , [Herbet Alves de Oliveira](#) , [Cochiran Pereira dos Santos](#) ,  
[Maria de Andrade Gomes](#) , [Mário Ernesto Giroldo Valério](#) , [Zélia Soares Macedo](#) \*

Posted Date: 2 April 2025

doi: [10.20944/preprints202504.0209.v1](https://doi.org/10.20944/preprints202504.0209.v1)

Keywords: Eco-friendly brick; Soil-cement; Gypsum waste; Sustainable materials



Preprints.org is a free multidisciplinary platform providing preprint service that is dedicated to making early versions of research outputs permanently available and citable. Preprints posted at Preprints.org appear in Web of Science, Crossref, Google Scholar, Scilit, Europe PMC.

Copyright: This open access article is published under a Creative Commons CC BY 4.0 license, which permit the free download, distribution, and reuse, provided that the author and preprint are cited in any reuse.

Disclaimer/Publisher's Note: The statements, opinions, and data contained in all publications are solely those of the individual author(s) and contributor(s) and not of MDPI and/or the editor(s). MDPI and/or the editor(s) disclaim responsibility for any injury to people or property resulting from any ideas, methods, instructions, or products referred to in the content.

## Article

# Sustainable Use of Gypsum Waste for Applications in Soil-Cement Bricks: Mechanical, Environmental, and Durability Performance

Elvia Soraya Santos Nascimento<sup>1</sup>, Herbet Alves de Oliveira<sup>2</sup>, Cochiran Pereira dos Santos<sup>3</sup>, Maria de Andrade Gomes<sup>4</sup>, Mário Ernesto Giroldo Valério<sup>1</sup> and Zélia Soares Macedo<sup>1,\*</sup>

<sup>1</sup> Postgraduate Program in Materials Science, Federal University of Sergipe, São Cristóvão, SE, Brazil; elviadorasaya@academico.ufs.br, zelia.macedo@academico.ufs.br, megvalerio@academico.ufs.br

<sup>2</sup> Department of Civil Engineering, Federal Institute of Sergipe, Aracaju, SE, Brazil; herbet.oliveira@ifs.edu.br

<sup>3</sup> Physics Department, Federal University of Sergipe, São Cristóvão, SE, Brazil; cochiran@academico.ufs.br

<sup>4</sup> Federal University of Sergipe; mg.lpcmuhs@gmail.com

\* Correspondence: zelia.macedo@academico.ufs.br

**Abstract:** This study explores the use of gypsum waste from civil construction as a partial replacement for cement in soil-cement formulations, aiming to produce eco-friendly bricks aligned with circular economy principles. Formulations were prepared using a 1:8 cement-to-soil ratio, with gypsum replacing cement in proportions ranging from 5% to 40%. The raw materials were characterized in terms of their chemical composition, crystalline phases, plasticity, and thermal profile. The formulations, molded by uniaxial pressing into cylindrical bodies and cured for 7 or 28 days, were tested for crystalline phases, compressive strength, water absorption, durability, and microstructure. Water absorption remained below 20% for all samples, with an average value of 16.20%. Compressive strength after 7 days decreased slightly with increasing gypsum content, from 16.36 MPa (0% gypsum) to 13.74 MPa (40% gypsum), still meeting the quality standard. After 28 days of curing, the formulation containing 10% gypsum achieved the highest strength (26.7 MPa), surpassing the reference sample without gypsum (25.2 MPa). Mass loss due to water immersion remained within acceptable limits for formulations containing up to 20% gypsum. Notably, samples with 5% and 10% gypsum exhibited superior mechanical performance, while samples with 20% gypsum showed comparable results to the reference. These findings suggest that replacing up to 20% of cement with gypsum waste is a viable and sustainable alternative, promoting circular economy practices and reducing the environmental impact of construction waste.

**Keywords:** eco-friendly brick; soil-cement; gypsum waste; sustainable materials

## 1. Introduction

In recent years, sustainable practices have gained prominence across various sectors, driven by the urgent need to preserve natural resources and mitigate environmental impacts. The concept of sustainable development, as defined by the United Nations (UN) World Commission on Environment and Development in 1983, emphasizes the importance of meeting present needs without compromising the ability of future generations to meet their own. Achieving this goal requires managing key elements in production chains, including reducing natural resource consumption, minimizing energy use, decreasing waste generation, and promoting material reuse and recycling. Solid waste management, in particular, plays an important role in advancing the UN's Sustainable Development Goals (SDGs), especially SDG 11 (Sustainable Cities and Communities), SDG 12 (Responsible Consumption and Production), and SDG 13 (Climate Action). Effective waste management strategies can significantly enhance sustainability by fostering resource recovery through circular economy principles [1,2].

The construction sector stands out as one of the most impactful industries due to its intensive consumption of raw materials and substantial waste generation. According to Vilela [3], the industry has increasingly sought innovative and creative approaches to integrate sustainability into all phases of production, aiming to reduce resource use and environmental impact. A notable advancement is the development of eco-friendly construction materials, such as soil-cement bricks, which offer a sustainable and cost-effective alternative to conventional materials. These bricks, composed primarily of soil and cement, are simple to produce and can be manufactured on-site, significantly reducing logistical costs [4].

The eco-efficiency of soil-cement bricks is determined by their environmental impact, resource utilization, and performance characteristics. Key indicators of eco-efficiency include the use of locally sourced materials, reduced energy consumption, a smaller carbon footprint, and favorable mechanical properties. Utilizing locally available soil minimizes transportation needs and associated environmental impacts [4]. Furthermore, incorporating engineering waste and recycled fine aggregates enhances eco-efficiency by promoting waste reuse and reducing landfill contributions [5]. In assessing the environmental impact of a product, it is important to evaluate not only its quantity but also its quality or performance. The method used to evaluate these ecological consequences provides a comprehensive view of the product's sustainability [6].

In terms of energy consumption and carbon footprint, soil-cement bricks require significantly less energy than traditional fired bricks, as they do not undergo kiln firing [7]. Life cycle assessments reveal that these bricks have a lower carbon footprint compared to ceramic and concrete blocks, making them a more sustainable choice for masonry construction [8]. They also exhibit adequate compressive strength and durability, meeting the necessary standards for construction use [5,9]. Optimal mix proportions for eco-friendly unfired clay bricks, including soil-cement variants, ensure desirable mechanical properties while maintaining environmental compatibility [5].

Despite these advantages, challenges remain in optimizing production processes and material properties to further enhance the sustainability of soil-cement bricks. Research has explored the incorporation of various waste materials, such as coffee husks, paper and pulp industry waste, sugarcane bagasse ash, and leather powder, with mixed results. For instance, Castro et al. [10] found that coffee husk particles reduced compressive strength and durability while increasing water absorption. Conversely, Azevedo et al. [11] demonstrated that paper and pulp industry waste could improve internal filling, reducing porosity and the final weight of the bricks. Araújo et al. [12] also confirmed the feasibility of using sugarcane bagasse ash and leather powder in soil-cement brick production.

One underexplored waste material in this context is gypsum, which is a major byproduct of civil construction, particularly from projects using flue gas desulfurization (FGD) gypsum, a residue from thermal power plants that remove sulfur dioxide ( $\text{SO}_2$ ). In 2020, global FGD gypsum production reached 255 million tons, with Asia accounting for 55% of the total, followed by Europe (22%) and North America (18%) [13]. In Brazil, 1.3 million tons of gypsum are produced annually, primarily in the Araripe Gypsum Center in Pernambuco State [14]. However, improper handling leads to significant waste, with studies indicating that up to 47% of gypsum used in coatings is discarded [15]. Recycling gypsum waste is challenging due to sulfate contamination, which can hinder reuse and generate harmful emissions in landfills [16]. Responsible management of this waste is crucial to avoid resource depletion, and to mitigate environmental and public health risks. Recent studies such as those by Hashim et al. [6] and Antunes et al. [17] demonstrate that waste gypsum and ceramic residues can significantly enhance the sustainability of construction materials, supporting circular economy goals. The scientific and technological innovation of using gypsum lies in its potential to optimize the mechanical and physical performance of soil-cement specimens by altering their microstructure and enhancing hydration and carbonation properties. Unlike other additives, such as pozzolans and fibers, which primarily improve long-term strength and durability, gypsum can enhance both initial strength and dimensional stability.

Considering these facts, the present study aims to produce and characterize soil-cement brick specimens incorporating gypsum waste from civil construction. The research seeks to determine the maximum amount of gypsum that can replace cement while maintaining the mechanical properties

and durability of the bricks within established standards. This work contributes to advancing knowledge on the technical and environmental feasibility of using gypsum waste in construction materials, aligning with circular economy principles and the UN Sustainable Development Goals (SDGs).

## 2. Materials and Methods

### 2.1. Raw Materials

The selected soil is a highly plastic clay rich in limestone, commonly used in ceramic tile production. After collection, the soil was dried in an oven at  $60 \pm 5$  °C. Grain size analysis was conducted according to ASTM D6913/D6913M [18], and the specific density of the soil was measured following DNER-ME-093/94 [19]. Plastic properties, including liquid limit (LL), plastic limit (PL), and plasticity index (PI), were determined in accordance with ASTM D4318 [20].

The cement used was CP V-ARI, characterized through the following tests: setting time ASTM C191 [21], specific gravity ASTM C188 [22], specific surface area NBR 16372, using the Blaine permeability method [23], and compressive strength ASTM C109/C109M, [24]. These tests evaluated hydration initiation, density, surface area, and mechanical strength under load, respectively.

The gypsum waste, sourced from residues generated by companies producing and installing residential gypsum boards, has the chemical formula  $\text{CaSO}_4 \cdot 0.5\text{H}_2\text{O}$ . In construction, gypsum is mixed with water in specific proportions to achieve its setting properties, transforming into  $\text{CaSO}_4 \cdot 2\text{H}_2\text{O}$ . The collected waste was reduced to a particle size of approximately 1 cm, dried at  $60 \pm 5$  °C to remove moisture that could hinder sieving, and then ground in a ball mill. The resulting powder was sieved through an ASTM No. 100 sieve (150  $\mu\text{m}$ ) and stored in airtight containers to protect it from environmental exposure [25].

### 2.2. Characterization Techniques

X-ray diffraction (XRD) patterns of the cement, gypsum, and soil samples were obtained using a Rigaku DMAX 100 diffractometer with  $\text{CuK}\alpha 1$  radiation ( $\lambda = 1.5418$  Å). Scans were performed in continuous mode over a 20 range of 5° to 70° at a scan rate of 1°/min. The crystalline phases were identified by comparing experimental patterns with the ICSD crystallographic database.

The morphology of the soil-cement composites after 28 days of curing was analyzed using a JEOL JSM-6510LV scanning electron microscope (SEM) at CMNANO/UFS (Proposal 082026P073). The SEM operated at 15 kV in secondary electron imaging (SEI) mode. Chemical composition analysis was performed using energy-dispersive X-ray spectroscopy (EDX) with an EDX-7000 spectrometer under vacuum, using a 10 mm collimator and Mylar capsule. Operating conditions included voltages of 50 kV (Al-U) and 15 kV (Na-Sc), with a 100 s acquisition time and ~30% dead time.

Thermogravimetric analysis (TGA) of the soil was conducted using a TA Instruments SDT Q600 under a nitrogen atmosphere. Approximately 10 mg of sample was heated in a platinum crucible at a rate of 10 °C/min from room temperature to 1000 °C. Quantitative chemical composition was determined using energy-dispersive X-ray fluorescence (EDXRF) with a Shimadzu EDX-7000 spectrometer.

### 2.3. Mechanical and Durability Testing

After curing the specimens for 7 and 28 days in a sheltered environment, they were subjected to compressive strength, water absorption, and specific density tests following NBR 8492 [26]. Durability was assessed through wetting and drying cycles in accordance with NBR 13554 [27].

### 2.4. Statistical Analysis

The normality of the data was verified, and an analysis of variance (ANOVA) was performed to evaluate the influence of waste incorporation percentages on the properties of the soil-cement bricks. Statistical analysis was conducted using Paleontological Statistics (PAST) software, with a significance level (p-value) of  $\leq 0.05$ , followed by Tukey's test [28].

### 2.5. Physical and Chemical Characterization of Raw Materials

Table 1 presents the values of specific density, bulk density, and specific surface area of the raw materials. A soil with a high specific mass, such as 2.71 g/cm<sup>3</sup>, indicates that its constituent minerals have a high intrinsic density. This suggests the presence of heavy minerals, such as quartz or iron oxides, which contribute to a dense and robust structure. Soils with high specific gravity typically exhibit lower porosity, which can directly influence mechanical strength [29]. For cement and sand, the obtained values are consistent with standard ranges for these materials.

Regarding specific surface area, the values for cement and soil are similar, while the gypsum residue exhibits a significantly higher value. The larger specific surface area of gypsum indicates smaller and more uniformly distributed particles. This characteristic can significantly influence the properties of cementitious composites, affecting hydration, mechanical strength, and durability [30].

**Table 1.** Physical characterization of raw materials.

	Specific (g.cm <sup>3</sup> )	Gravity	Bulk (g.cm <sup>3</sup> )	Density	Specific (cm <sup>2</sup> /g)	Surface Area
Soil	2,71 ± 0,02		1,15 ± 0,01		4243 ± 100	
Gypsum	2,25 ± 0,02		1,10 ± 0,02		5500 ± 150	
Cement	3,10 ± 0,02		1,40 ± 0,02		4400 ± 120	
Sand	2,63 ± 0,01		1,65 ± 0,01		-	

Table 2 provides the chemical composition of the soil, cement, sand, and gypsum, obtained through EDX analysis. According to Alves et al. [31], the physical and chemical characterization of soil is essential to determine its suitability for producing eco-friendly bricks. The soil should contain a sand fraction to ensure stability and a controlled amount of clay to promote cohesion and efficient cement hydration. The soil is predominantly composed of silica (SiO<sub>2</sub> – 39.39%), with lower percentages of calcium oxide (CaO – 22.97%), iron oxide (Fe<sub>2</sub>O<sub>3</sub> – 18.45%), and alumina (Al<sub>2</sub>O<sub>3</sub> – 9.40%). Similar compositions have been reported in previous studies [32], which are associated with clay minerals, quartz, and feldspars, as well as the presence of limestone [33]. The SiO<sub>2</sub>/Al<sub>2</sub>O<sub>3</sub> ratio of 4.33 is higher than the typical values for kaolinite (1.18) or montmorillonite (2.36) [34], indicating a higher proportion of free quartz and accessory minerals. Elevated levels of alkaline oxides (Na<sub>2</sub>O + K<sub>2</sub>O) suggest the presence of feldspars (KAlSi<sub>3</sub>O<sub>8</sub>) or mica [35]. The high CaO content indicates the presence of carbonates. Silica reduces plasticity but aids in the drying process, while alumina enhances thermal stability, plasticity, and structural performance [36]. Iron oxide (Fe<sub>2</sub>O<sub>3</sub>) improves mechanical properties, such as strength and reduced plasticity, by acting as a binding agent that increases particle cohesion [37].

In the cement analysis, calcium oxide (CaO – 80.95%) predominates, with smaller fractions of silica (SiO<sub>2</sub> – 8.46%) and iron oxide (Fe<sub>2</sub>O<sub>3</sub> – 5.95%). Sand is primarily composed of silica (SiO<sub>2</sub> – 89.79%), while gypsum consists mainly of calcium oxide (CaO – 68.01%) and sulfur trioxide (SO<sub>3</sub> – 29.97%).

**Table 2.** Chemical composition of raw materials (% by mass).

Component	Soil	Cement	Sand	Gypsum
CaO	22.97	80.95	1.54	68.01
SiO <sub>2</sub>	39.39	8.46	89.79	0.63
Fe <sub>2</sub> O <sub>3</sub>	18.45	5.95	1.721	-
SO <sub>3</sub>	0.11	2.06	0.32	29.97
K <sub>2</sub> O	6.95	1.60	0.66	0.30
Al <sub>2</sub> O <sub>3</sub>	9.40	-	1.82	-
TiO <sub>2</sub>	2.09	0.37	3.56	-
Loss on ignition	0.64	0.61	0.59	1.09

## 2.6. X-ray Diffraction (XRD) Analysis of Raw Materials

The X-ray diffraction (XRD) patterns of the raw materials used in the production of soil-cement bricks with gypsum addition are illustrated in Figure 1. The diffractogram of the cement revealed characteristic peaks of alite (tricalcium silicate,  $3\text{CaO}\cdot\text{SiO}_2$  or  $\text{C}_3\text{S}$ ) and larnite (dicalcium silicate,  $2\text{CaO}\cdot\text{SiO}_2$  or  $\text{C}_2\text{S}$ ), two of the main anhydrous phases of Portland cement [38]. The crystallographic references used were: Cement (ICSD: 162744; 169890; 39006), Gypsum (ICSD: 161625; 040043), and Soil (ICSD: 89280; 166966; 169911).

The XRD pattern of the gypsum powder (Figure 2) indicated that the sample is predominantly composed of calcium sulfate hemihydrate ( $\text{CaSO}_4\cdot0.5\text{H}_2\text{O}$ ), representing 80.8% of the composition. This phase is particularly relevant due to its ability to react with water to form calcium sulfate dihydrate ( $\text{CaSO}_4\cdot2\text{H}_2\text{O}$ ) [39]. The analysis also identified 19.2% calcium sulfate dihydrate, confirming the material's significance in reactive systems. Additionally, peaks corresponding to anhydrous calcium sulfate were detected, a significant component in calcined raw gypsum ore, commonly used as construction gypsum [40,41].

The XRD analysis of the soil revealed quartz as the most abundant mineral, ranging from 30.8% to 61.7%. According to Carvalho et al. [42] and Celik [35], quartz is primarily associated with granular particles and exhibits low physicochemical activity. As a result, quartz has a minor role in moisture retention but contributes to reduce plasticity. Another clay mineral identified was illite, which has higher plasticity than kaolinite and a crystalline structure similar to montmorillonite [35].

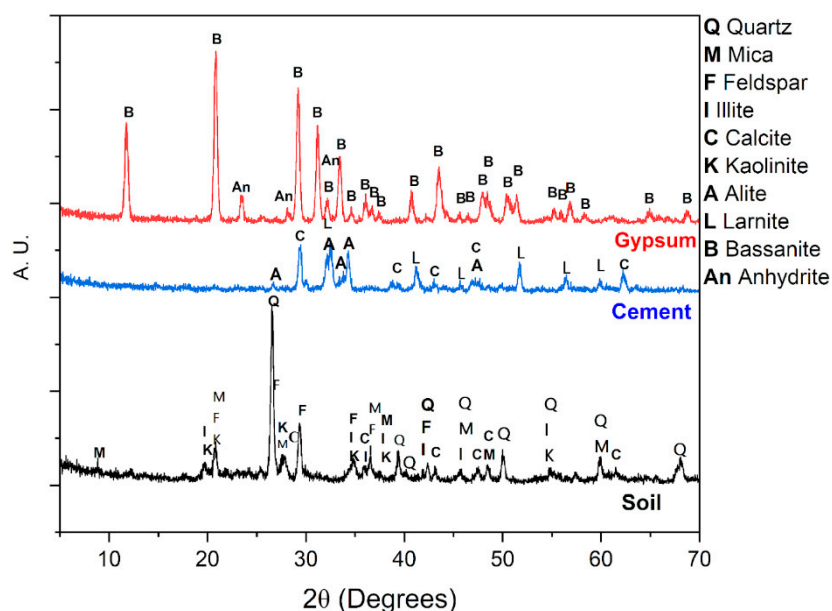


**Figure 1.** X-ray diffraction (XRD) patterns of the composite components.

## 2.7. Particle Size Distribution of Raw Materials

The particle size distribution of the raw materials is presented in Figure 2. Particle size is a critical factor in the strength of soil-cement bricks, as it directly affects compaction and the interaction between mixture components, such as soil, cement, and water. Smaller particles, like clays, increase cohesion due to their larger surface area, facilitating cement hydration reactions, while larger particles, such as sand, contribute to structural stability by acting as a granular skeleton. A balanced particle size distribution improves particle packing, reducing internal voids and increasing density, which enhances compressive strength and reduces water absorption. Mixtures with an appropriate proportion of fine (less than 0.075 mm) and coarse particles optimize the performance of soil-cement bricks, combining cohesion and mechanical strength [43].

The particle size distributions of cement, gypsum, and soil were analyzed. According to ABCP (1985) and NBR 10833 [44], soils suitable for producing soil-cement bricks must meet the following

criteria: 100% of the soil must pass through a No. 4 sieve (4.8 mm), and 10% to 50% of the sample must pass through a No. 200 sieve (0.075 mm). As shown in Figure 2, all materials passed 100% through the No. 4 sieve (4.8 mm). For the No. 200 sieve (0.075 mm), cement and soil passed approximately 40%, while gypsum passed about 10%. Therefore, all materials meet the granulometric classification requirements.

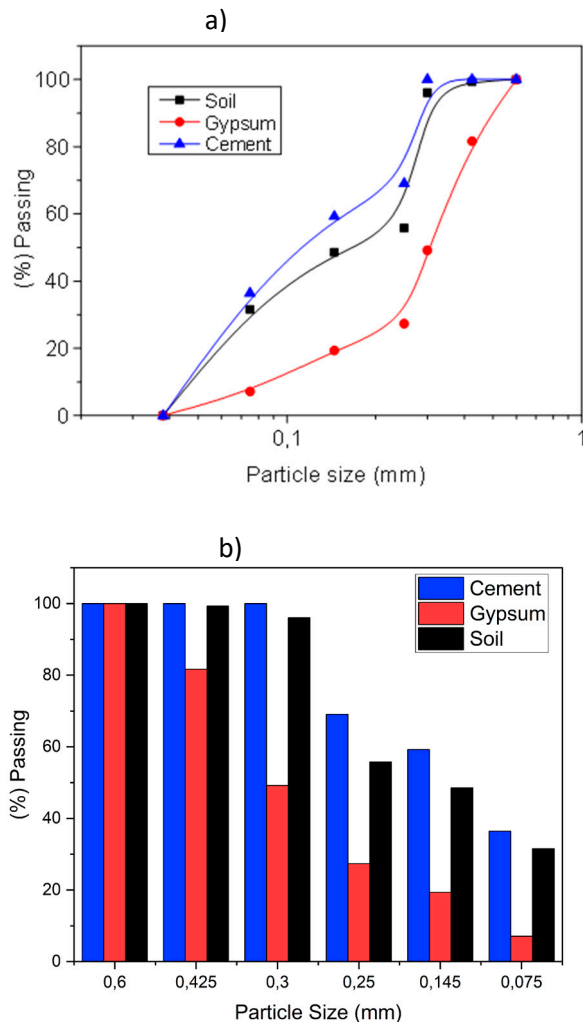


**Figure 2.** (a) Particle size distribution of the soil-cement brick components, obtained through granulometric testing according to ASTM D6913/D6913M (ASTM, 2017); (b) Histogram of particle size distribution.

### 2.8. Soil Plasticity and Thermal Analysis of Gypsum and Soil

The plasticity index (PI) of the soil was 8.0, and the liquid limit (LL) was 32%, classifying it as medium plasticity, which is considered suitable for soil-cement brick production [45,46]. According to ABCP (1985) and NBR 10833 [44], the liquid limit should be less than 45%, and the plasticity index should be less than 18%. Therefore, the soil meets the requirements. This soil falls within the range of inorganic clays of low plasticity (CL) under the Unified Soil Classification System (USCS) and belongs to the A-2-6 group in the Transportation Research Board (TRB) system. These are granular soils with clayey fine fractions that influence plastic behavior. Such soils are moderately cohesive and exhibit good compaction when properly moistened. The compressive strength of cement-stabilized soils decreases significantly with increasing PI due to the less efficient formation of cementitious materials like calcium silicate hydrate (CSH) and other compounds that fill soil pores [47]. Soils with higher PI exhibit lower density of these materials, leading to reduced compaction and, consequently, lower mechanical strength [47].

Figure 3 presents the TG/DTG curve of gypsum, revealing two main mass loss peaks. The first peak, at 139 °C, is likely related to the partial loss of water, consistent with the partial dehydration of gypsum and its conversion to hemihydrate described in previous studies [48,49]. Between 90 °C and

140 °C, gypsum undergoes a continuous transformation, including the formation of hemihydrate before reaching the anhydrite phase, completing the transition above 170 °C [50]. This process can be influenced by the presence of acids and salts, which accelerate or delay the transformation [51]. Above 180 °C, the transformation from anhydrite III to anhydrite II begins. The formation of anhydrite from gypsum depends significantly on temperature and environmental conditions. Generally, anhydrite begins to form when gypsum is exposed to temperatures above 42 °C under low humidity, representing a precise estimate for the transition point from gypsum to anhydrite, considering the slow crystallization kinetics of anhydrite below 90 °C [52]. Other studies indicate that anhydrite formation can occur at temperatures as low as 35 °C in the presence of microbial organic substances, suggesting that microbial processes can influence anhydrite mineralization in specific environments [53]. Another event, of lower intensity, was identified in the TG/DTG curve in Figure 3, near 560 °C, suggesting the presence of thermally active components not identified in the XRD analysis, possibly due to the decomposition of impurities of gypsum. Comparing the TG/DTG curve with the EDS results, these events may be associated with the thermal decomposition of contaminant oxides in the gypsum sample, as described in Table 2. Studies by Engbrecht & Hirschfeld [54] found that gypsum undergoes thermal decomposition of carbonate components, such as calcite and dolomite, around 700 °C, a phenomenon not detected in the XRD analysis. Another hypothesis for the discrete events observed in Figure 4 is the possible evaporation of residual water in the gypsum crystal structure, leading to anhydrite formation, as suggested by [55].

Figure 4 presents the TG/DTG curve of the soil, showing a small mass loss below 120 °C, primarily attributed to the evaporation of free water, i.e., water not associated with exchangeable cations or present between clay particles. Between 120 °C and 430 °C, the mass loss was related to the release of water bound to exchangeable cations. In the range of 430 °C to 600 °C, mass reduction occurred due to the dehydration of clay minerals, such as aluminum silicate. Between 600 °C and 800 °C, the dehydration of calcium silicate occurs. Similar results have been reported in other studies investigating the impact of polymer treatment on soil properties [56].

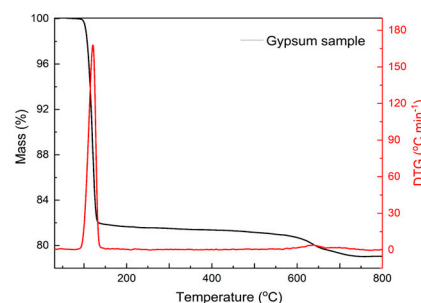


**Figure 3.** Thermogravimetric analysis and its first derivative (TG/DTG) of gypsum.

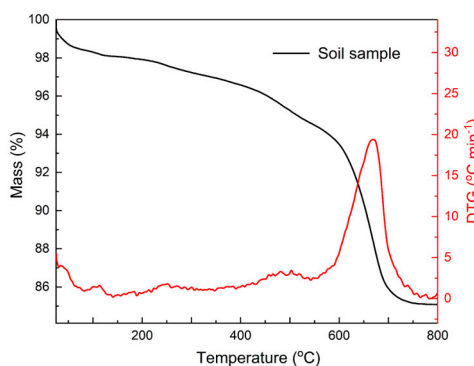


**Figure 4.** Thermogravimetric analysis and its first derivative (TG/DTG) of soil.

## 2.9. Preparation and Testing of Soil-Cement Formulations

The formulations initially tested contained 90 % soil and 10 % cement. Since this mixture did not achieve the minimal mechanical strength specified by the standard (which is 2 MPa), a partial substitution of the soil by fine aggregate (sand) was used. Specimens of 200 g were uniaxially pressed into cylindrical shapes with approximate dimensions of 6 cm in diameter and 4 cm in height, maintaining a moisture content of 10%, as established in the literature [45, 43, 46, 57, 58]. Figure 5 presents the mechanical strength of specimens pressed under 5 MPa, 10 MPa or 15 MPa, with partial substitution of soil by sand. The results indicated that the mixture of 10 % sand, 80 % soil and 10 % cement, pressed under 10 MPa, provided the best mechanical strength of the specimens.

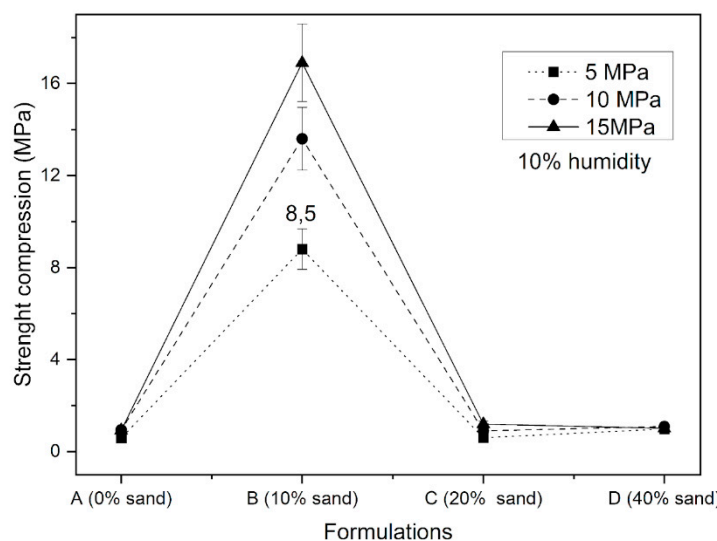


**Figure 5.** Mechanical strength of the formulations containing 10 % cement and sand proportion varying from 0 % to 40 % of the total mass, substituting the soil.

In this study, the specimens were air-cured under the natural environmental conditions of the state of Sergipe, Brazil. Given the regional climate, characterized by an average annual temperature of approximately 25°C and a relative humidity ranging from 70% to 82%, no humidification system was used.

After molding, the specimens were stored in a sheltered environment, protected from direct sunlight and wind, as recommended by NBR 8492 [26]. This method aligns with common construction industry practices and ensures a systematic evaluation of the curing process under real climatic conditions. The impact of air curing on soil-cement bricks has been studied by several researchers. Edike et al. [59] found that air-cured bricks exhibited progressive strength development over time, despite the lower efficiency of cement hydration compared to wet curing. The influence of curing temperature on the strength of cementitious bricks has been widely studied. Research indicates that both curing temperature and humidity play a crucial role in the mechanical strength development of these materials. For instance, studies on charcoal-based bricks have shown that higher curing temperatures (40 °C) promote greater early strength at 7 days, whereas lower temperatures (20 °C), combined with high humidity (90%), result in improved strength at 28 days [60].

Furthermore, studies on hybrid cements containing granulated blast furnace slag and fly ash indicate that curing temperatures in the range of 50–60 °C accelerate initial hydration, leading to higher early-age strength. However, this effect may be counterproductive in the long term, as it can result in heterogeneous formation of hydration products and coarser porosity, negatively impacting the final strength of the material [61].

Hu et al. [62] investigated the effects of drying and wetting cycles on stabilized soils, emphasizing the need to protect air-cured bricks from direct sunlight to minimize shrinkage cracks.

The specimens were tested at 7 and 28 days to assess their mechanical properties. Five formulations were prepared, incorporating varying proportions of gypsum residue as a partial cement substitute. The formulations were categorized based on their gypsum content, as presented in Table 3. Samples without gypsum were designated as SF (standard formulation) for reference. These measures ensured a structured analysis of the effects of gypsum substitution and curing conditions on brick strength.

**Table 3.** Compositions of the formulations used in the experiments (%).

Compositio ns	Soil	Ceme nt	Sand	Gyps u m
SF	80	10	10	-
G5	80	9.5	10	0.5
G10	80	9	10	1
G20	80	8	10	2
G40	80	6	10	4

Compressive strength evaluation after 7 and 28 days of curing were performed to assess their axial load-bearing capacity. The compressive strength test was carried out using a Contenco HD-200T hydraulic press, with a maximum capacity of 200 tons (2000 kN). The test specimens were cylindrical, with a diameter of 62.3 mm and a height of 32.1 mm, molded according to the applicable standards NBR 12025 [63]. The loading rate was maintained between 1.0 MPa/s and 1.5 MPa/s, as recommended by the corresponding standard NBR 5739 [64]. The measurements were repeated for five specimens of each formulation. Water absorption and density were determined after 28 days of curing, using three specimens of each formulation. In this procedure, the dry mass (M) was initially registered, then the samples were immersed in distilled water for 24 hours and weighed again to provide the wet mass (Mw). The water absorption corresponds to the difference between the wet and dry mass NBR 10836 [65]. The apparent density was determined as  $D_b = M/V$ , where the volume V was obtained from the direct measurement of the high and diameter, with precision of 0.02 mm. Durability tests were performed with three specimens of each formulation and consisted in a simulation of weather conditions, through alternating wetting and drying cycles. For this, the specimens were immersed in water for 6 hours and then dried for 18 hours in an oven at a controlled temperature of 70°C. The mass of the specimen was recorded before and after this cycle, and six consecutive cycles were performed, as specified in NBR 8492 [26].

### 3. Results

The results obtained from the X-Ray Diffraction (XRD) analysis revealed the proportions of the different phases present in the analyzed materials, determined using the Match! software (demo version).

**Table 4.** Proportions of the phases identified by XRD using the Match! software.

Mineral Phase	Concentration Range (%)
Quartz	24,7 - 38,0
Paragonite	18,4 - 22,8
Inesite	10,1 - 15,8

Mineral Phase	Concentration Range (%)
Ettringite	8,0 - 10,0
Calcite	12,5 - 16,2
Gypsum	0,9 - 2,5
Ilite	16,9 - 20,1

The absence of portlandite ( $\text{Ca}(\text{OH})_2$ ) in X-ray diffraction (XRD) analysis may be attributed to various chemical and mineralogical factors. The high silica ( $\text{SiO}_2$ ) content in the soil (39.39%, as determined using the Match! software, demo version) promotes pozzolanic reactions, consuming portlandite to form cementitious compounds such as C-S-H (calcium silicate hydrate) and C-A-S-H (calcium aluminum silicate hydrate), thereby reducing its detection [66]. The presence of alumina ( $\text{Al}_2\text{O}_3$ , 9.40%) and iron oxide ( $\text{Fe}_2\text{O}_3$ , 18.45%) suggests the formation of hybrid cementitious phases, such as C-A-F-H, which also consume portlandite [67]. Furthermore, the high  $\text{CaO}$  content in the soil (22.97%) indicates the presence of carbonates, which may have reacted with portlandite through carbonation, converting it into calcite ( $\text{CaCO}_3$ ) [68].

Portlandite may also be present in an amorphous or low-crystallinity form, making its detection by XRD challenging, thus requiring complementary techniques such as thermogravimetric analysis (TGA) for confirmation [69]. Another relevant factor is carbonation, where portlandite reacts with atmospheric  $\text{CO}_2$ , forming calcite ( $\text{CaCO}_3$ ), whose presence is observed in the diffractograms in Figure 6, potentially masking or replacing the characteristic portlandite peaks in XRD [70]. Calcium carbonate precipitation preferably occurs around clay particles and other materials in the system, contributing to the evolution of the material's mechanical properties [71]. Calcite is widely found in cementitious materials containing calcium-rich residues, reinforcing its relevance in the context of sustainability and material reuse [72, 73]. Therefore, the absence of portlandite in XRD does not indicate its inexistence but rather its consumption in chemical reactions, highlighting the complexity of transformations in the soil-cement system.

The cement hydration process is inherently complex, mainly due to the formation of products such as C-S-H (calcium silicate hydrate) and C-A-S-H (calcium aluminum silicate hydrate), which exhibit significant variability in their chemical compositions and are often nearly amorphous. This amorphous nature makes their identification challenging in XRD analyses. Variability in  $\text{Ca}/\text{Si}$  molar ratios and the presence of disordered structures further complicate precise detection by XRD. Recent studies highlight that C-S-H can exist in various forms, ranging from nanocrystals to highly disordered structures [74]. Additionally, advanced techniques such as liquid-cell transmission electron microscopy reveal that C-S-H growth occurs through a complex nucleation mechanism, forming structures that are not fully crystalline but exhibit nanocrystalline regions within an amorphous matrix [75].

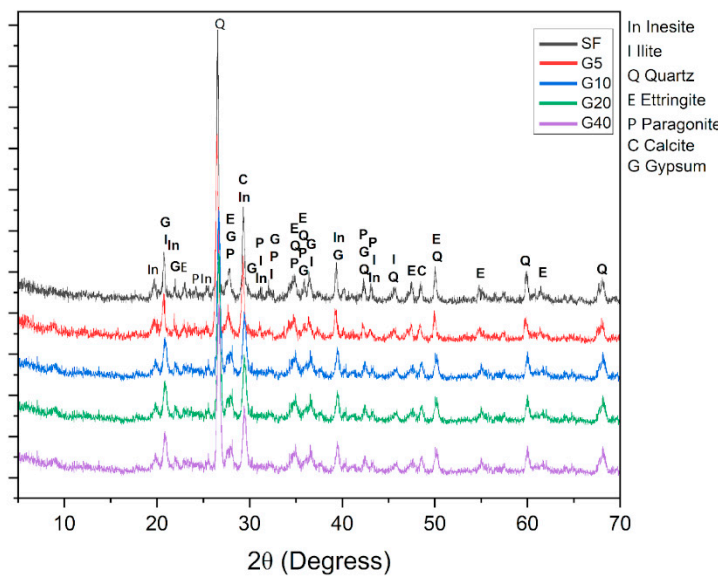


**Figure 6.** X-ray diffraction of the formulations.

Figure 7 presents the water absorption results for all the samples. The analyses were carried out after 7 days of curing, and the results indicate a slight enhance of water absorption from  $(15.71 \pm 0.5)$  % to  $(16.54 \pm 1)$  % as the gypsum content goes from zero to 40 % substituting the cement mass. Despite this increase, all the values stayed below 20 %, which is the maximum allowed by NBR 10834 [76], for 7-days cured samples. Using analysis of variance (ANOVA), we can confirm that the results show a significant difference between the means, as the F-value (332.80) exceeds the critical F-value (5.3176), and the p-value  $(8.38 \times 10^{-8})$  is much lower than 0.05. This indicates that the observed variations are statistically significant and unlikely to have occurred by chance. However, the residue-containing samples present water absorption that comply with the standard, although slightly higher than the result obtained for the standard formulation. The water absorption of soil-cement bricks is directly related to porosity and pore connectivity [77]. The high silica ( $\text{SiO}_2$ ) content in the soil (39.39%, as determined by XRD results) and the formation of C-S-H gel (calcium silicate hydrate) contribute to the densification of the material's microstructure, reducing pore connectivity and, consequently, water absorption. On the other hand, the chemical reaction of cement with the aluminosilicates present in the soil generates cementitious products, such as calcium silicate hydrate (C-S-H) and calcium aluminosilicate hydrate (C-A-S-H), which bind the soil particles and solidify over time, minimizing pore interconnectivity [78,79]. With the partial replacement of cement by gypsum, there will be a lower proportion of these cementitious compounds, explaining the slight increase in water absorption observed in gypsum-based formulations.

The obtained density values reveal no significant variations among the formulations, with values of  $(1.95 \pm 0.01)$   $\text{g/cm}^3$  determined for all formulations. This result is justified since cement represents only 10% of the formulation; thus, replacing 40% of the cement with gypsum corresponds to a 4% change in the total composition. As a result, the density remained within the quality criteria established by the NBR 10834 standard [76].

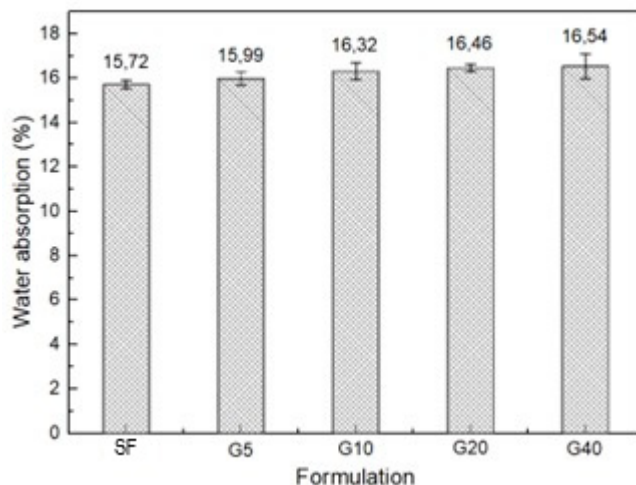


**Figure 7.** Water absorption of the specimens cured for 7 days.

Compressive strength after curing for 7 or 28 days is shown in Figure 8. Statistical analysis confirmed that the variation among the means is significant, with  $F = 199.0166$ —well above the critical  $F$ -value of 5.3176—and  $p = 6.1947E-07$ , which is far below the 0.05 threshold. Mechanical strength is a key parameter, as the bonding force between clay particles can be influenced by their interaction with cement and gypsum. Clays have a layered structure with fine particles that enhance cohesion through Van der Waals forces and cation exchange between layers. This cohesion is critical to the initial strength of the bricks. Excess gypsum may affect this bonding, since gypsum expands when bassanite crystals ( $\text{CaSO}_4 \cdot 0.5\text{H}_2\text{O}$ ) are hydrated to form gypsum ( $\text{CaSO}_4 \cdot 2\text{H}_2\text{O}$ ), potentially reducing contact and cohesion between the clay and cement particles [80]. The presence of gypsum clusters could also contribute to a decrease in mechanical strength [81]. Therefore, controlling the gypsum content is essential to maintain the mechanical integrity of soil-cement bricks. As shown in Figure 8, the mechanical strength of all formulations remained above 13 MPa, far exceeding the 2 MPa minimum required, indicating that the gypsum content used in this study is safe from a mechanical performance standpoint. After 28 days of curing, sample G10, containing 10% gypsum, reached an average strength of 26.5 MPa—about 6% higher than the 25.2 MPa observed for the standard formulation (SF). Substitutions beyond this percentage led to reductions of up to 20% (with 20 MPa recorded for G40), while still remaining above the required standard. During cement hydration, the primary compounds formed are calcium silicate hydrate (C-S-H) and ettringite, as described by Cai et al. [82] and confirmed in this study through XRD analysis. According to Hu et al. [62], cement contains free  $\text{CaO}$ , which reacts with water to form  $\text{Ca}(\text{OH})_2$ . This compound interacts with  $\text{CaSO}_4$  from the gypsum in the cement, delaying the setting time. Moreover, in the presence of cement aluminates, this reaction promotes additional ettringite formation, contributing to early strength development. However, when gypsum waste ( $\text{CaSO}_4 \cdot \text{H}_2\text{O}$ ) is used as a partial replacement for cement, the lack of free  $\text{CaO}$ —potentially consumed during earlier reactions—causes the excess calcium sulfate to behave as an inert material. This impairs the formation of new hydration products, resulting in reduced strength development. Other factors, such as increased porosity due to less efficient particle packing, may also contribute to decreased mechanical strength. Nevertheless, all formulations demonstrated satisfactory compressive strength, meeting the quality requirements.

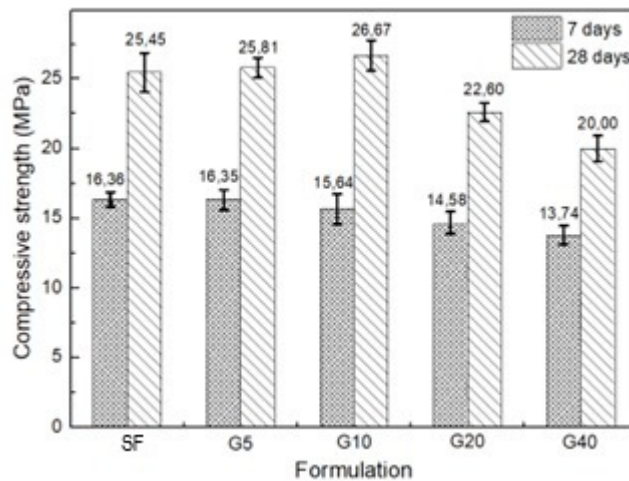


**Figure 8.** Compressive strength of the specimens after curing for 7 and 28 days.

Figure 9 shows the durability results of the specimens cured for 28 days and evaluated based on mass loss after six wetting and drying cycles. The results for samples SF, G5, G10, and G20 stayed below the 10% limit established by NBR 13553 [83] for A-2-6 group soils in the TRB system. However, the G40 formulation exhibited mass loss of approximately 23.86%, standing out of the quality requirements. One of the factors that may negatively impact durability is the formation of ettringite ( $\text{Ca}_6\text{Al}_2(\text{SO}_4)_3(\text{OH})_{12}\cdot26\text{H}_2\text{O}$ ), which results from the reaction between tricalcium aluminate ( $\text{C}_3\text{A}$ ) and sulfates present in gypsum. In moderate amounts, ettringite can contribute to early strength gain by filling pores and reducing the material's permeability [84]. However, when sulfate levels are excessive, the continuous formation of ettringite can lead to expansion and internal cracking, compromising the structural integrity of the material. Gu et al. [85] demonstrated that although ettringite initially forms in larger pores without causing significant expansion, its intrusion into smaller capillary pores can accelerate swelling, resulting in structural damage and reduced durability. On the other hand, the high presence of silica ( $\text{SiO}_2$ ) and alumina ( $\text{Al}_2\text{O}_3$ ) in the soil promotes the formation of more stable phases, such as calcium silicate hydrate (C-S-H) and calcium-aluminum-silicate hydrate (C-A-S-H) gels. These compounds are less susceptible to leaching and contribute to microstructural densification, enhancing both strength and durability. The formation of these compounds is particularly important in formulations with lower gypsum content, where the pozzolanic reaction between silica, alumina, and cement is more effective, resulting in a more durable material.

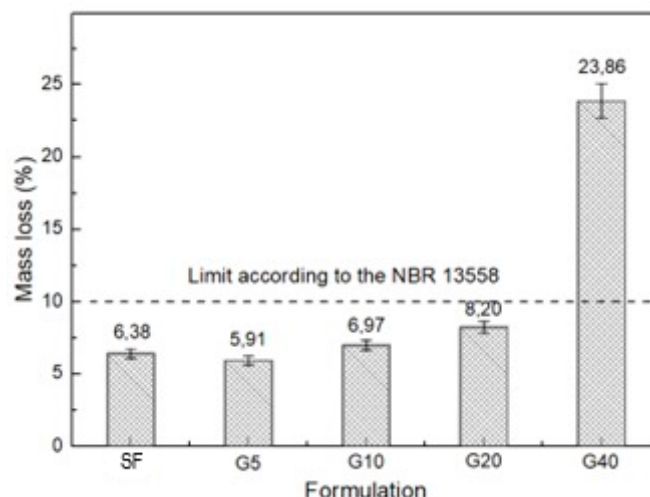


**Figure 9.** Durability of the specimens cured for 28 days, evaluated by mass loss after six wetting and drying cycles.

The analysis of the scanning electron microscopy (SEM) images revealed that the microstructure of the SF sample (Fig. 10a) exhibits a homogeneous and densified matrix, with good cohesion among the soil, sand, and hydrated cement components, reflecting efficient cement hydration. In the sample containing 10% gypsum (Fig. 10b), SEM analysis revealed a heterogeneous microstructure with calcium-rich regions. This technique allows for the observation of the morphology of hydration products, such as possible formations associated with C-S-H and ettringite. However, the definitive identification of these crystalline phases requires complementary techniques, such as X-ray diffraction (XRD), which had previously indicated their presence (Fig. 6). This microstructure suggests a balance between cement hydration and the formation of secondary phases, which may contribute to the material's mechanical performance [86].

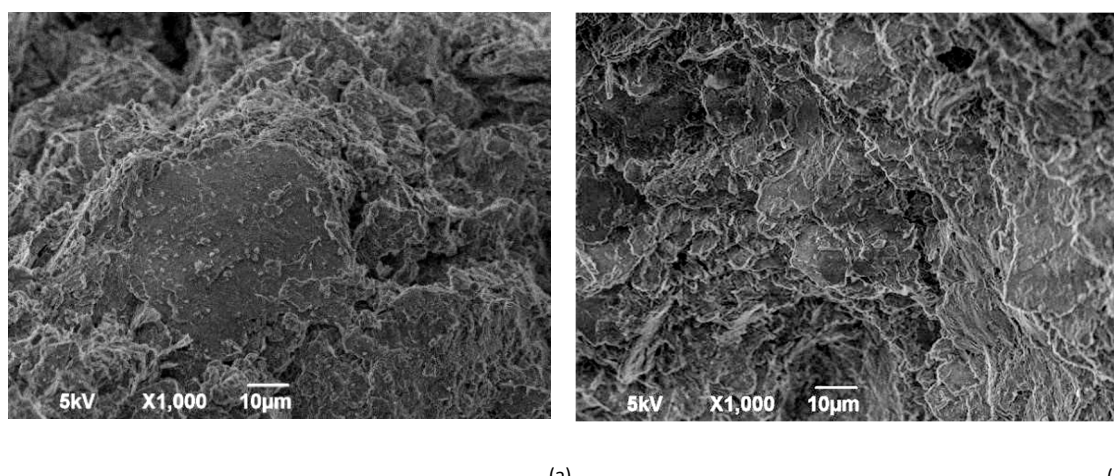
The energy-dispersive spectroscopy (EDS) analysis of the G10 sample (Fig. 11b) highlighted the effective distribution of calcium (Ca), silicon (Si), and aluminum (Al), indicating the formation of a dense and stable cementitious matrix. These elements are associated with the formation of cementitious phases such as C-S-H and calcium-alumino-silicate hydrates (C-A-S-H), which are fundamental to mechanical strength and material durability. The presence of these phases explains the improved mechanical performance observed in the formulation with 10% gypsum, where the formation of a structured and cohesive network contributed to microstructural stability.

In contrast, the sample with 40% gypsum (Fig. 10c) presented a less cohesive matrix, with higher porosity and visible cracking, indicating a disruption in the formation of cementitious phases. The irregular distribution of elements such as iron (Fe), aluminum (Al), silicon (Si), magnesium (Mg), and sodium (Na), as shown in the EDS analysis (Fig. 11c), suggests the presence of residual soil minerals and incomplete hydration products. This microstructural discontinuity correlates with the reduced mechanical strength, higher water absorption, and increased mass loss observed in this formulation.

The absence of portlandite ( $\text{Ca}(\text{OH})_2$ ) in the XRD analysis supports the hypothesis that carbonation processes may have consumed part of the portlandite, leading to the formation of calcite ( $\text{CaCO}_3$ ) and an increase in material porosity. The excessive incorporation of gypsum compromises the microstructural integrity of the material, primarily due to the overproduction of ettringite ( $\text{Ca}_6\text{Al}_2(\text{SO}_4)_3(\text{OH})_{12}\cdot 26\text{H}_2\text{O}$ ). While moderate amounts of ettringite can fill pores and enhance early strength, excessive concentrations may cause volumetric expansion and cracking, thereby reducing durability.

Furthermore, the presence of free quartz, as evidenced by the high molar ratio  $\text{SiO}_2/\text{Al}_2\text{O}_3$  (ranging from 8.66 to 10.53, calculated based on the proportions of crystalline phases identified by XRD using the Match! software), may act as an inert phase, creating discontinuity zones within the cementitious matrix, which promote pore formation and increase water absorption.

The EDS spectrum (Fig. 11) showed spectral lines consistent with the chemical composition data presented in Table 2, confirming the expected presence of elements in the formulations. Finally, the absence of portlandite in the XRD analysis suggests that the pozzolanic reaction may have been incomplete, leaving unreacted silica and alumina, which may explain the higher porosity and reduced strength in the formulations with higher gypsum content.



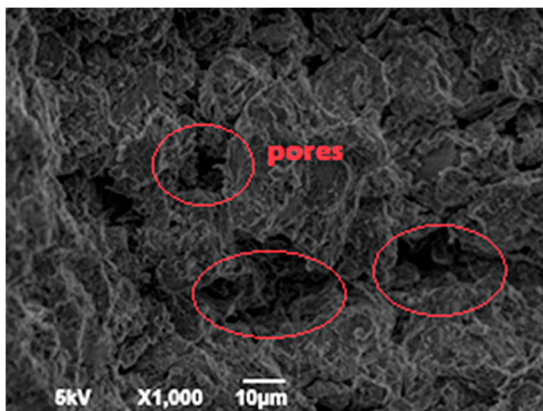


**Figure 10.** SEM micrographs of the fracture surface of soil-cement specimens cured for 28 days: a) SF; b) G10; c) G40.

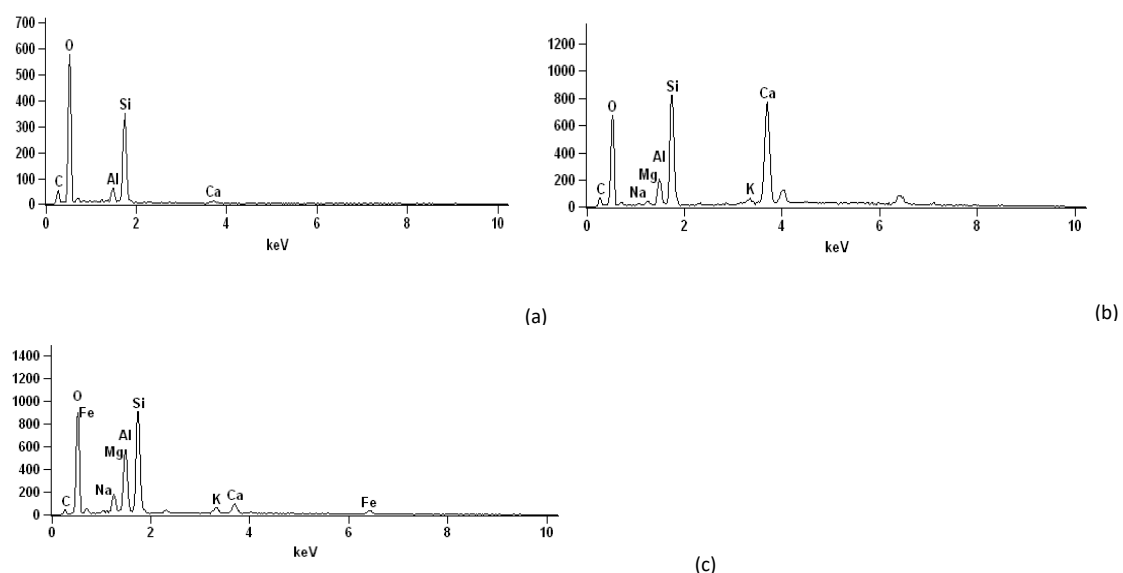


**Figure 11.** EDS spectra of the fracture surface of soil-cement specimens cured for 28 days: a) SF; b) G10; c) G40.

## 5. Conclusions

The results demonstrated that replacing up to 20% of the cement mass with gypsum waste does not significantly compromise the performance of the bricks. All tested formulations met the requirements of Brazilian technical standards. The 10% gypsum formulation (G10), in particular, showed superior compressive strength after 28 days of curing compared to the reference sample. This improvement was attributed to the formation of denser cementitious matrices, rich in C-S-H and C-A-S-H phases, as supported by microstructural (SEM/EDS) and mineralogical (XRD) analyses.

Water absorption increased slightly with higher gypsum contents due to the rise in porosity; however, all values remained below the 20% threshold defined by NBR 10834 [76]. Similarly, durability was preserved in samples with up to 20% gypsum, as evidenced by mass loss within acceptable limits after wetting and drying cycles. The 40% gypsum formulation (G40), however, showed significantly reduced durability, linked to excessive ettringite formation and premature carbonation.

Importantly, this study reinforces the environmental and economic benefits of utilizing construction waste. The partial replacement of cement with gypsum waste contributes to the reduction of raw material consumption, diverts significant volumes of gypsum from landfills, and aligns with circular economy strategies. Furthermore, it supports the Sustainable Development Goals (SDGs) by promoting responsible resource use, reducing the carbon footprint of construction materials, and minimizing environmental impact.

In conclusion, the incorporation of up to 20% gypsum waste in soil-cement bricks is a viable and sustainable alternative, offering both technical performance and ecological advantages. However, proportions above this threshold should be avoided due to their detrimental effects on durability and microstructural stability.

**Acknowledgments:** The authors express their gratitude to CAPES and CNPq for the financial support, which was essential for conducting this research. They also thank the Soil and Materials Laboratories of the Federal Institute of Sergipe (IFS), the CMNANO of the Federal University of Sergipe (UFS), and LMDCEM – Multiuser Laboratories of the Department of Materials Science and Engineering, for providing the infrastructure and technical support that were fundamental for carrying out the experiments and analyses.

## References

1. Mariyam, S.; et al. A framework to support localized solid waste management decision making: Evidence from Qatar. *Environ. Dev.* **2024**, *50*, 100986. <https://doi.org/10.1016/j.envdev.2024.100986>.
2. Beccarello, M.; Di Foggia, G. Sustainable Development Goals data-driven local policy: Focus on SDG 11 and SDG 12. *Adm. Sci.* **2022**, *12*(4), 167. <https://doi.org/10.3390/admsci12040167>.
3. Vilela, A. P.; et al. Technological properties of soil-cement bricks produced with iron ore mining waste. *Constr. Build. Mater.* **2020**, *262*, 120883. <https://doi.org/10.1016/j.conbuildmat.2020.120883>.
4. Silva, M. V. V. da; et al. Técnicas de estabilização e reforço sustentável do solo. *Rev. FT* **2024**, *29*(141), 29–30. <https://doi.org/10.69849/revistaft/ar10202412061929>.
5. Xiong, W.; et al. Reuse of engineering waste soil and recycled fine aggregate to manufacture eco-friendly unfired clay bricks: Experimental assessment, data-driven modeling and environmental friendliness evaluation. *Case Stud. Constr. Mater.* **2023**, *19*, e02608. <https://doi.org/10.1016/j.cscm.2023.e02608>.
6. Hashim, A. A.; et al. Improving the mechanical, corrosion resistance, microstructural and environmental performance of recycled aggregate concrete using ceramic waste powder as an alternative to cement. *Ceramics* **2025**, *8*(1), 11. <https://doi.org/10.3390/ceramics8010011>.
7. **Rocha Silva, B.; et al.** Soil cement brick production process: Literature review. *MOJ Civil Engineering* **2023**, *7*(1), 19–26. <https://doi.org/10.15406/mojce.2023.07.00169>.
8. Leão, A. S.; et al. Is the soil-cement brick an ecological brick? An analysis of the life cycle environmental and energy performance of masonry walls. *Sustainability* **2022**, *14*(19), 12735. <https://doi.org/10.3390/su141912735>.
9. Ângelo, F. A.; Simões, G. F. Tijolos ecoeficientes de barro cru com resíduos sólidos e efluente industrial utilizando tecnologias não convencionais. *Ambiente Construído* **2023**, *23*(2), 1–15. <https://doi.org/10.1590/s1678-86212023000200667>.
10. Castro, E. D. de; et al. Analysis of the coffee peel application over the soil-cement bricks properties. *Coffee Science* **2019**, *14*(1), 12. <https://doi.org/10.25186/cs.v14i1.1503>.
11. Azevedo, A. R. G. et al. Assessing the potential of sludge generated by the pulp and paper industry in assembling locking blocks. *Journal of Building Engineering* **2019**, *23*, 334–340. <https://doi.org/10.1016/j.jobe.2019.02.012>.
12. Araújo, V. D. et al. Incorporation of tannery waste and sugarcane bagasse ash in soil-cement bricks. *Revista AIDIS de Ingeniería y Ciencias Ambientales* **2022**, *15*(1), 154. <https://doi.org/10.22201/iingen.0718378xe.2022.15.1.77053>.
13. Ahmed, A.; Ugai, K.; Kamei, T. Laboratory and field evaluations of recycled gypsum as a stabilizer agent in embankment construction. *Soils and Foundations* **2011**, *51*(6), 975–990. <https://doi.org/10.3208/sandf.51.975>.
14. Azevedo, A. C. et al. Adhesion of gypsum plaster coatings: Experimental evaluation. In *Building Pathology and Rehabilitation* (pp. 41–66); Springer: 2021. [https://doi.org/10.1007/978-3-030-74406-3\\_3](https://doi.org/10.1007/978-3-030-74406-3_3).
15. Camarini, G.; Pimentel, L. L.; De Sá, N. H. R. Assessment of the material loss in walls renderings with  $\beta$ -hemihydrate paste. *Applied Mechanics and Materials* **2011**, *71*–78, 1242–1245. <https://doi.org/10.4028/www.scientific.net/AMM.71-78.1242>.

16. Jiménez-Rivero, A.; García-Navarro, J. Exploring factors influencing post-consumer gypsum recycling and landfilling in the European Union. *Resources, Conservation and Recycling* **2017**, *116*, 116–123. <https://doi.org/10.1016/j.resconrec.2016.09.014>.
17. Antunes, M. L. P. et al. Utilization of gypsum from construction and demolition waste in Portland cement mortar. *Cerâmics* **2019**, *65*(Suppl 1), 1–6. <https://doi.org/10.1590/0366-6913201965s12588>.
18. ASTM International. ASTM D6913: Standard test methods for particle-size distribution (gradation) of soils using sieve analysis. West Conshohocken, PA: ASTM International, 2017.
19. Departamento Nacional de Estradas de Rodagem (DNER). DNER-ME 093/94: Solos – Determinação da Densidade Real. Rio de Janeiro: DNER, 1994.
20. ASTM International. ASTM D4318-18: Standard Test Methods for Liquid Limit, Plastic Limit, and Plasticity Index of Soils. West Conshohocken, PA: ASTM International, 2018.
21. ASTM International. ASTM C191: Standard test methods for time of setting of hydraulic cement by Vicat needle. West Conshohocken, PA: ASTM International, 2023.
22. ASTM International. ASTM C188: Standard test method for density of hydraulic cement. West Conshohocken, PA: ASTM International, 2022.
23. Associação Brasileira de Normas Técnicas. NBR 16372:2015 – Cimento Portland e outros materiais em pó – Determinação da finura pelo método de permeabilidade ao ar (método de Blaine). ABNT, 2015.
24. ASTM International. ASTM C109/C109M: Standard test method for compressive strength of hydraulic cement mortars. West Conshohocken, PA: ASTM International, 2023.
25. Krejsová, J. et al. New insight into the phase changes of gypsum. *Materials and Structures* **2024**, *57*(5). <https://doi.org/10.1617/s11527-024-02404-z>.
26. Associação Brasileira de Normas Técnicas. NBR 8492: Tijolo de solo-cimento – Análise dimensional, determinação da resistência à compressão e da absorção de água – Método de ensaio. ABNT, 2012.
27. Associação Brasileira de Normas Técnicas. NBR 13554: Solo-cimento – Ensaio de durabilidade por molhagem e secagem – Método de ensaio. ABNT, 2012.
28. Vieira, S. Análise de variância ANOVA (1<sup>a</sup> ed.). Editora Atlas, 2006.
29. Mitchell, J. K., & Soga, K. Fundamentals of soil behavior, 3rd ed.; John Wiley & Sons: Hoboken, NJ, USA, 2005.
30. Chernyshova, N. et al. Enhancement of fresh properties and performances of the eco-friendly gypsum-cement composite (EGCC). *Construction and Building Materials* **2020**, *260*, 120462. <https://doi.org/10.1016/j.conbuildmat.2020.120462>.
31. Alves, M. N. de L. X. de F.; Barros, S. V. A.; de Oliveira, F. N. Physical and chemical characterization of soil for use in ecological bricks. In *Uniting Knowledge Integrated Scientific Research For Global Development*, Vol. 2; Seven Editora: São Paulo, 2024.
32. Costa Gonçalves, L. F. Da; Balestra, C. E. T.; Ramirez Gil, M. A. Evaluation of mechanical, physical and chemical properties of ecological modular soil-alkali activated bricks without Portland cement. *Environmental Development* **2023**, *48*, 100932. <https://doi.org/10.1016/j.envdev.2023.100932>
33. Alcântara, A. C.; Beltrão, M. S.; Oliveira, H. A.; Gimenez, I. F.; Barreto, L. S. Characterization of ceramic tiles prepared from two clays from Sergipe-Brazil. *Appl. Clay Sci.* **2008**, *39*, 160–165. <https://doi.org/10.1016/j.clay.2007.05.010>.
34. Boussen, S.; Sghaier, D.; Chaabani, F.; Jamoussi, B.; Bennour, A. Characteristics and industrial application of the Lower Cretaceous clay deposits (Bouhedma Formation), southeast Tunisia: Potential use for the manufacturing of ceramic tiles and bricks. *Applied Clay Science* **2016**, *123*, 210–221. <https://doi.org/10.1016/j.clay.2016.01.027>
35. Celik, H. Technological characterization and industrial application of two Turkish clays for the ceramic industry. *Applied Clay Science* **2010**, *50*, 245–254. <https://doi.org/10.1016/j.clay.2010.08.014>
36. Egole, C. P.; Medupin, R. O.; Nzebuka, G. C.; Nnodum, N. A.; Ochieze, U. P.; Eterigho-Ikelegbe, O.; Wilson, U. N.; & Yoro, K. O. Quartz and feldspar-blended clay composites for thermal and structural applications. *Results in Materials* **2024**, *23*, 100584. <https://doi.org/10.1016/j.rinma.2024.100584>

37. Sridharan, A., Sudhakar, M. R., Ramanath, K. P., & Nagaraj, H. B. The role of iron hydroxide in the engineering behaviour of tropical soils. *Geotechnics in the African Environment*, **2022**, 7–14. <https://doi.org/10.1201/9781003241155-2>

38. Harrison, T., Jones, M. R., & Lawrence, D. The production of low energy cements. In *Lea's Chemistry of Cement and Concrete* (p. 341–361). Elsevier, **2019**.

39. Reigl, S. et al. Toward more sustainable hydraulic binders: Controlling calcium sulfate phase selection via specific additives. *ACS Sustainable Chemistry & Engineering*, **2023**, 11(23), 8450–8461. <https://doi.org/10.1021/acssuschemeng.3c00429>

40. Buryanov, A. F. et al. Research on the influence of gypsum and anhydrite stone impurities on the properties of the binder. In *Lecture Notes in Civil Engineering* (pp. 138–146). Springer, **2021**. [https://doi.org/10.1007/978-3-030-72404-7\\_13](https://doi.org/10.1007/978-3-030-72404-7_13)

41. Stawski, T. M. et al. Nucleation pathway of calcium sulfate hemihydrate (bassanite) from solution: Implications for calcium sulfates on mars. *The Journal of Physical Chemistry C*, **2020**, 124(15), 8411–8422. <https://doi.org/10.1021/acs.jpcc.0c01041>

42. Carvalho, J. C. de et al. (Eds.). *Solos não saturados no contexto geotécnico*. ABMS, **2023**. <https://doi.org/10.4322/978-65-992098-3-3>

43. Ashour, T., Korjenic, A., & Korjenic, S. Equilibrium moisture content of earth bricks biocomposites stabilized with cement and gypsum. *Cement and Concrete Composites*, **2015**, 59, 18–25. <https://doi.org/10.1016/j.cemconcomp.2015.03.005>

44. Associação Brasileira de Normas Técnicas. *NBR 10833: Fabricação de tijolo e bloco de solo-cimento com utilização de prensa manual ou hidráulica - Procedimento*. Rio de Janeiro: ABNT, **2012**.

45. Rosa, J. M. de S. S., Silva, R. G. P. da, & Lafayette, K. P. V. Sustainable alternative for the production of soil cement bricks. *Journal of Management and Sustainability*, **2023**, 13(1), 45. <https://doi.org/10.5539/jms.v13n1p45>

46. Metzker, S. L. O. et al. Soil-cement bricks development using polymeric waste. *Environmental Science and Pollution Research*, **2022**, 29(14), 21034–21048. <https://doi.org/10.1007/s11356-021-16769-z>

47. Bian, X. et al. Plasticity role in strength behavior of cement-phosphogypsum stabilized soils. *Journal of Rock Mechanics and Geotechnical Engineering*, **2022**, 14(6), 1977–1988. <https://doi.org/10.1016/j.jrmge.2022.01.003>

48. Krause, F. et al. Reactivity of gypsum-based materials subjected to thermal load: Investigation of reaction mechanisms. *Materials*, **2020**, 13(6), 1427. <https://doi.org/10.3390/ma13061427>

49. Ritterbach, L., & Becker, P. Temperature and humidity dependent formation of  $\text{CaSO}_4 \cdot x\text{H}_2\text{O}$  ( $x = 0 \dots 2$ ) phases. *Global and Planetary Change*, **2020**, 187, 103132. <https://doi.org/10.1016/j.gloplacha.2020.103132>

50. Kyono, A. et al. Structural evolution of gypsum ( $\text{CaSO}_4 \cdot 2\text{H}_2\text{O}$ ) during thermal dehydration. *Journal of Mineralogical and Petrological Sciences*, **2022**, 117(1). <https://doi.org/10.2465/jmps.220811>

51. Azimi, G., & Papangelakis, V. G. Mechanism and kinetics of gypsum–anhydrite transformation in aqueous electrolyte solutions. *Hydrometallurgy*, **2011**, 108(1–2), 122–129. <https://doi.org/10.1016/j.hydromet.2011.03.007>

52. Voigt, W., & Freyer, D. Solubility of anhydrite and gypsum at temperatures below 100 °C and the gypsum–anhydrite transition temperature in aqueous solutions: A re-assessment. *Frontiers in Nuclear Engineering*, **2023**, 2. <https://doi.org/10.3389/fnuen.2023.1208582>

53. Al Disi, Z. A. et al. Microbially influenced formation of anhydrite at low temperature. *The Science of the Total Environment*, **2023**, 902, 165820. <https://doi.org/10.1016/j.scitotenv.2023.165820>

54. Engbrecht, D. C., & Hirschfeld, D. A. Thermal analysis of calcium sulfate dihydrate sources used to manufacture gypsum wallboard. *Thermochimica Acta*, **2016**, 639, 173–185. <https://doi.org/10.1016/j.tca.2016.07.021>

55. Lira, M. C. de A., & Neiva, L. S. Investigative study of the potentialities of noble applications for the Brazilian calcium sulfate  $\alpha$ -hemihydrate. *Pesquisa e Ensino em Ciências Exatas e da Natureza*, **2020**, 4, 01. <https://doi.org/10.29215/pecen.v4i0.1516>

56. Vipulanandan, C., & Mohammed, A. XRD and TGA, swelling and compacted properties of polymer treated sulfate contaminated CL soil. *Journal of Testing and Evaluation*, **2016**, 44(6), 2270–2284. <https://doi.org/10.1520/JTE20140280>

57. Kongkajun, N., Laitila, E. A., Ineure, P., Prakaypan, W., Cherdhirunkorn, B., & Chakartnarodom, P. Soil-cement bricks produced from local clay brick waste and soft sludge from fiber cement production. *Case Studies in Construction Materials*, 2020, 13, e00448. <https://doi.org/10.1016/j.cscm.2020.e00448>

58. Leonel, R. F., Folgueras, M. V., Dalla Valentina, L. V. O., Prim, S. R., Prates, G. A., & Caraschi, J. C. Characterization of soil-cement bricks with incorporation of used foundry sand. *Cerâmica*, 2017, 63(367), 329–335. <https://doi.org/10.1590/0366-69132017633672131>

59. Edike, U. E., Ameh, O. J., & Dada, M. O. Performance of polymer bricks produced with plastic waste. *Innovative Infrastructure Solutions*, 2023, 8(1). <https://doi.org/10.1007/s41062-022-01021-5>

60. Kumar, R., Patel, K., & Singh, B. New coal char-based bricks: Effects of curing temperature, humidity, pressing pressure, and addition of superplasticizer on physical, mechanical, and thermal properties. *OSTI.gov*. 2023. Disponível em: <https://www.osti.gov/pages/biblio/2279157>.

61. Zhao, X., Wang, Y., & Li, J. Hydration characteristics of hybrid cements containing granulated blast furnace slag and fly ash at elevated curing temperatures. *Frontiers in Materials*. 2022. Disponível em: <https://www.frontiersin.org/journals/materials/articles/10.3389/fmats.2022.982568/full>.

62. Hu, W. et al. Effects of wetting–drying cycles on the macro and micro properties of the cement-stabilized soil with curing agent. *Buildings*, 2024, 14(6), 1716. Disponível em: <https://doi.org/10.3390/buildings14061716>.

63. Associação Brasileira de Normas Técnicas. 2012. NBR 12025: Solo-cimento – Ensaio de compressão simples de corpos de prova cilíndricos – Método de ensaio. ABNT.

64. Associação Brasileira de Normas Técnicas. 2007. NBR 5739: Cimento Portland – Determinação da resistência à compressão. ABNT.

65. Associação Brasileira de Normas Técnicas. 2012. NBR 10836: Bloco de solo-cimento sem função estrutural – Análise dimensional, determinação da resistência à compressão e da absorção de água – Método de ensaio. ABNT.

66. Macioski, G., Soto, N. T. A., Medeiros, M. H. F. de, Hoppe Filho, J., Araújo, M. S. de, & Cerri, J. A. 2021. Portlandite consumption by red ceramic waste due to alkali activation reaction. *Ambiente Construído*, 21(1), 7–21. <https://doi.org/10.1590/s1678-86212021000100490>

67. Wild, S., & Khatib, J. M. 1997. Portlandite consumption in metakaolin cement pastes and mortars. *Cement and Concrete Research*, 27(1), 137–146. [https://doi.org/10.1016/s0008-8846\(96\)00187-1](https://doi.org/10.1016/s0008-8846(96)00187-1)

68. Kleib, J., Amar, M., Aouad, G., Bourbon, X., Benzerzour, M., & Abriak, N.-E. 2022. The use of Callovo-Oxfordian Argillite as a raw material for Portland cement clinker production. *Buildings*, 12(9), 1421. <https://doi.org/10.3390/buildings12091421>

69. Al-Tabbaa, A., Yi, Y. L., Liska, M., & Unluer, C. 2013. Initial investigation into the carbonation of MgO for soil stabilisation. *Cement and Concrete Research*, 53, 1–9. <https://doi.org/10.1016/j.cemconres.2013.06.005>

70. Moon, D. H., Lee, J.-R., Grubb, D. G., & Park, J.-H. 2010. An assessment of Portland cement, cement kiln dust and Class C fly ash for the immobilization of Zn in contaminated soils. *Environmental Earth Sciences*, 61(8), 1745–1750. <https://doi.org/10.1007/s12665-010-0596-1>

71. Park, S.-S. et al. 2015. A study on soil cementation and calcite precipitation with clay as a medium. *Journal of the Korean Geotechnical Society*, 31(12), 17–27. <https://doi.org/10.7843/kgs.2015.31.12.17>

72. Siqueira, F. B., & Holanda, J. N. F. 2013. Reuse of grits waste for the production of soil-cement bricks. *Journal of Environmental Management*, 131, 1–6. <https://doi.org/10.1016/j.jenvman.2013.09.040>

73. Amaral, M. C. et al. 2013. Soil-cement bricks incorporated with eggshell waste. *Proceedings of the Institution of Civil Engineers - Waste and Resource Management*, 166(3), 137–141. <https://doi.org/10.1680/warm.12.00024>

74. Holmes, N., Tyrer, M., & Kelliher, D. 2022. Employing discrete solid phases to represent C-S-H solid solutions in the Cemdata07 thermodynamic database to model cement hydration using the PHREEQC geochemical software. *Applied Sciences*, 12(19), 10039. <https://doi.org/10.3390/app121910039>

75. Dong, P. et al. 2022. Liquid cell transmission electron microscopy reveals C-S-H growth mechanism during Portland cement hydration. *Materialia*, 22, 101387. <https://doi.org/10.1016/j.mtla.2022.101387>

76. Associação Brasileira de Normas Técnicas. 1994. NBR 10834: Tijolos solo-cimento - especificações. ABNT: Rio de Janeiro, Brasil.

77. Dulal, P.; X, Y.; Z, W. Engineering properties of cement-stabilized compressed earth bricks. *J. Build. Eng.* 2023, *77*, 107453. <https://doi.org/10.1016/j.jobe.2023.107453>
78. Thennarasan Latha, A.; Murugesan, B.; Thomas, B. S. Compressed stabilized earth block incorporating municipal solid waste incinerator bottom ash as a partial replacement for fine aggregates. *Buildings* 2023, *13*, 1114. <https://doi.org/10.3390/buildings13051114>
79. Corrêa-Silva, M.; X, Y.; Z, W. Constitutive behaviour of a clay stabilised with alkali-activated cement based on blast furnace slag. *Sustainability* 2022, *14*, 13736. <https://doi.org/10.3390/su142113736>
80. Zak, P.; X, Y.; Z, W. The influence of natural reinforcement fibers, gypsum and cement on compressive strength of earth bricks materials. *Constr. Build. Mater.* 2016, *106*, 179–188. <https://doi.org/10.1016/j.conbuildmat.2015.12.031>
81. Maichin, P.; X, Y.; Z, W. Stabilized high clay content lateritic soil using cement-FGD gypsum mixtures for road subbase applications. *Materials* 2021, *14*, 1858. <https://doi.org/10.3390/ma14081858>
82. Cai, H.; X, Y.; Z, W. Strength development of cemented soil cured in water-air conditions at varied temperatures: Experimental investigation and model characterization. *J. Mater. Civ. Eng.* 2023, *35*, 3. [https://doi.org/10.1061/\(ASCE\)MT.1943-5533.0004631](https://doi.org/10.1061/(ASCE)MT.1943-5533.0004631)
83. Associação Brasileira de Normas Técnicas. 2012. NBR 13553: Materiais para emprego em parede monolítica de solo-cimento sem função estrutural – Requisitos. ABNT: Rio de Janeiro, Brasil.
84. Höglund, L.O. Some notes of ettringite formation in cementitious materials; Influence of hydration and thermodynamic constraints for durability. *Cem. Concr. Res.* 1992, *22*, 217–228. [https://doi.org/10.1016/0008-8846\(92\)90059-5](https://doi.org/10.1016/0008-8846(92)90059-5)
85. Gu, Y.; X, Y.; Z, W. Pore size analyses of cement paste exposed to external sulfate attack and delayed ettringite formation. *Cem. Concr. Res.* 2019, *123*, 105766. <https://doi.org/10.1016/j.cemconres.2019.05.011>
86. Afflerbach, S.; Pritzel, C.; Hartwich, P.; Killian, M. S.; Krumm, W. Effects of thermal treatment on the mechanical properties, microstructure and phase composition of an ettringite-rich cement. *CEMENT* 2023, *11*, 100058. <https://doi.org/10.1016/j.cement.2023.100058>
87. in all publications are solely those of the individual author(s) and contributor(s) and not of MDPI and/or the editor(s). MDPI and/or the editor(s) disclaim responsibility for any injury to people or property resulting from any ideas, methods, instructions or products referred to in the content.

**Disclaimer/Publisher's Note:** The statements, opinions and data contained in all publications are solely those of the individual author(s) and contributor(s) and not of MDPI and/or the editor(s). MDPI and/or the editor(s) disclaim responsibility for any injury to people or property resulting from any ideas, methods, instructions or products referred to in the content.